

## Optimizing $T_1$ -weighted imaging of cortical myelin content at 3.0 T

Nicholas A. Bock<sup>a,\*</sup>, Eyesha Hashim<sup>a</sup>, Rafal Janik<sup>b</sup>, Norman B. Konyer<sup>c</sup>, Marcel Weiss<sup>d</sup>, Greg J. Stanisz<sup>b</sup>, Robert Turner<sup>d</sup>, Stefan Geyer<sup>d</sup>

<sup>a</sup> Medical Physics and Applied Radiation Sciences, McMaster University, Hamilton, Ontario, Canada

<sup>b</sup> Sunnybrook Health Sciences Centre, Department of Imaging Research, Toronto, Ontario, Canada

<sup>c</sup> Imaging Research Centre, St. Joseph's Healthcare Hamilton, Hamilton, Ontario, Canada

<sup>d</sup> Department of Neurophysics, Max Planck Institute for Human Cognitive and Brain Sciences, Leipzig, Germany

### ARTICLE INFO

#### Article history:

Accepted 18 September 2012

Available online 1 October 2012

#### Keywords:

Magnetic resonance imaging

Brain mapping

Cortex

Myelin

Human

### ABSTRACT

With increases in the sensitivity and resolution of anatomical MRI for the brain, methods for mapping the organization of the cerebral cortex by imaging its myelin content have emerged. This identifies major sensory and motor regions and could be used in studies of cortical organization, particularly if patterns of myelination can be visualized over the cortical surface robustly in individual subjects. The imaging problem is difficult, however, because of the relative thinness of the cerebral cortex and the low intracortical tissue contrast. In this paper, we optimize the contrast of  $T_1$ -weighted MRI to help better visualize patterns of myelination. We measure a small but statistically significant difference in  $T_1$  of  $171 \pm 40$  ms between cortical regions with low and high myelin contents in the human cortex at 3 T, and then perform simulations to choose parameters for an inversion-recovery pulse sequence that utilizes this  $T_1$  difference to increase contrast within the cortex. We show that lengthening the delay between signal acquisition and the next inversion pulse in the sequence increases intracortical contrast more effectively than does image averaging. Using the optimized sequence, we show that major myelinated regions that are relatively thick, such as the primary motor and auditory regions, can be visualized well in individuals at 3 T using whole-cortex 3D images made at 1 mm isotropic resolution, while thinner regions, such as the primary visual cortex, can be visualized using targeted 3D images made at 0.5 mm isotropic resolution. Our findings demonstrate that patterns of myelination can be better visualized in individual subjects when the imaging is optimized to highlight intracortical contrast and can help to pave the way for the creation of matched maps of microanatomy and function in the cortex of living individual humans.

© 2012 Elsevier Inc. All rights reserved.

### Introduction

The human cortex is highly organized and the location and boundaries of specific regions can be described using structural and functional measures. One emerging method to map the cortex *in vivo* based on its microstructure in humans and non-human primates is by imaging and mapping its myelin content (Bock et al., 2011; Cohen-Adad et al., 2012; Geyer et al., 2011; Glasser and Van Essen, 2011). While most myelinated axons in the brain are found in white matter tracts, there are a smaller number present throughout the cortex and the distribution and appearance of these fibers describe its myeloarchitecture. The feature of myeloarchitecture that is specifically imaged using MRI is the density of

radially and tangentially oriented myelinated fibers ascending to, descending from, and traversing the cortex. These myelinated fibers speed the conduction of input and output signals through the cortex and their density is regionally dependent. Indeed, it has long been known that specific sensory, motor, and associated regions of the human cortex can be identified by their high myelin content relative to their adjacent cortical tissue (Campbell, 1905; Elliott Smith, 1907; Hopf, 1955, 1956; Hopf and Vitzthum, 1957; Vogt and Vogt, 1919).

The ability to image patterns of cortical myelin content *in vivo* in humans is appealing, for it enables visualization of the location and extent of major cortical regions (including the primary somatosensory (S1), auditory (A1), visual (V1), and motor (M1) cortices). That ability will be useful for studies of cortical morphology (for example, the influence of age or sex on the size of cortical regions), and cortical plasticity (the influence of disease and rehabilitation on cortical organization), and for mapping the location of eloquent regions of the cortex prior to brain surgery or other invasive techniques. Moreover, the ability to image myelin content as an indicator of cortical microstructure is crucial for establishing a correspondence between structure and function in the human cortex. It would be ideal to image patterns of myelin

*Abbreviations:* S1, primary somatosensory cortex; A1, primary auditory cortex; V1, primary visual cortex; M1, primary motor cortex;  $T_1$ , longitudinal relaxation time;  $T_2$ , transverse relaxation time;  $T_2^*$ , effective transverse relaxation time; TI, inversion time; TD, segment delay time;  $B_1^-$ , receiver radiofrequency field in magnetic resonance imaging;  $B_1^+$ , transmitter radiofrequency field.

\* Corresponding author at: 1280 Main Street West, Hamilton, Ontario, Canada L8S 4K1. Fax: +1 905 522 5982.

E-mail address: [bockn@mcmaster.ca](mailto:bockn@mcmaster.ca) (N.A. Bock).

content robustly in individual subjects to best account for morphological variability and to enable patient studies; however, studies over the entire cortex in vivo have mostly relied on group measures to well reveal patterns (Cohen-Adad et al., 2012; Glasser and Van Essen, 2011), with individual maps proving less robust. Thus, there is a need for further improvement in the imaging procedure to improve its sensitivity and here we investigate optimizing image contrast. There has been a greater success in imaging myelin content patterns in targeted regions, such as V1 (Bridge et al., 2005; Geyer et al., 2011; Sánchez-Panchuelo et al., 2012), where coverage can be traded for improved image quality.

Imaging cortical myelin is based on the same MR contrast mechanism by which myelin in white matter tracts produces contrast between major gray and white matter structures of the brain. Reliably, it has been shown that the stripe of Gennari, a heavily myelinated structure in V1, can be identified on  $T_1$ -weighted (Barbier et al., 2002; Clare and Bridge, 2005),  $T_2$ -weighted (Carmichael et al., 2006; Trampel et al., 2011), and  $T_2^*$ -weighted images (Fukunaga et al., 2010). The contrast may also arise from non-heme iron in the cortex (Fukunaga et al., 2010), although this is co-localized with myelin, so its effect is to reinforce the same pattern seen when attempting to image cortical myelin.

Two factors make the imaging problem difficult. First, the amount of myelin in gray matter in the cortex is lower than in discrete white matter tracts. Hence, the difference in MRI parameters, such as  $T_1$  between cortical gray matter regions with low or high myelin content is much smaller than between cortical gray matter and white matter. Second, dense myelination is found over only some cortical layers, so that the thickness of myelinated cortex ranges only between 0.9 mm at its thinnest in S1 and 2.2 mm at its thickest in M1 (Zilles et al., 2012). (The overall thickness of the cortex in these regions ranges between 2.0 mm and 3.8 mm respectively (Fischl and Dale, 2000; Zilles et al., 2012).) This implies that a high resolution is needed for imaging to prevent loss of contrast from partial volumes of cerebral spinal fluid (CSF) or white matter encroaching on voxels containing cortical tissue. These two constraints dictate that anatomical imaging must be further optimized to generate good contrast within the cortex beyond any optimizations performed for whole-brain structural imaging.

In this paper, we develop anatomical imaging to reveal patterns of myelin density in individual subjects at a clinical MRI field strength of 3 T. Our approach is to acquire images based on  $T_1$ -contrast, because inversion-recovery  $T_1$ -weighted pulse sequences are particularly suited to high resolution 3D imaging (Deichmann et al., 2000, 2004). Another option would be  $T_2$ -weighted sequences optimized for high resolutions, such as Sampling Perfection with Application optimized Contrasts using different flip angle Evolutions (SPACE) (Lichy et al., 2005).  $T_2^*$  sequences may also be useful, but care may be needed in interpreting contrast arising from myelinated fibers, as this may depend on the relative orientation of the cortical sheet and the main magnetic field, due to the anisotropic magnetic susceptibility of myelinated axons (Cohen-Adad et al., 2012; Li et al., 2012).

For  $T_1$ -weighted imaging, we optimize a magnetization-prepared rapidly acquired gradient echo (MP-RAGE) pulse sequence (Mugler and Brookeman, 1990), one step of which is shown in Fig. 1. The sequence consists of a  $180^\circ$  inversion pulse, followed by an inversion time delay, TI, then a segment of a fast low-angle shot (FLASH) acquisition lasting a duration  $\tau$ . There is then another time delay, TD, to allow for partial spin relaxation, after which the sequence is repeated. Typically, TI is optimized to produce contrast based on the evolution of the longitudinal magnetization following the  $180^\circ$  pulse (labeled as  $M_{z1}$  in Fig. 1). To further improve contrast, we lengthen TD, which allows the longitudinal magnetization,  $M_{z2}$ , of a given tissue to relax more fully towards the equilibrium condition following the FLASH segment and prior to the next  $180^\circ$ .

For the optimization, we first measure  $T_1$  values in the brain at 3 T, then use those values in simulations of the MP-RAGE signal to find the optimum imaging parameters for producing good intracortical contrast. We use the optimized sequence to image the brain and show that thick

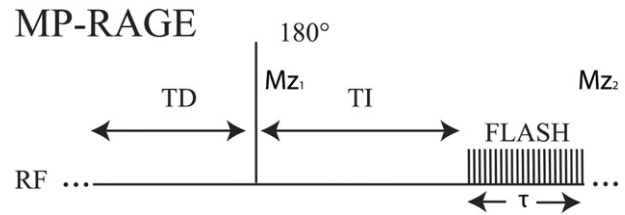


Fig. 1. The acquisition of one FLASH segment in an MP-RAGE pulse sequence.

major myelinated regions in individual subjects can be reliably identified, in clinically acceptable imaging times, at 3 T in 3D images with 1 mm isotropic resolution. Thinner regions can be identified in targeted 3D imaging of specific cortical regions at an isotropic resolution of 0.5 mm.

## Methods

### Subjects

$T_1$  measurements were obtained in five healthy female volunteers. The experiments were approved by the Research Ethics Board at Saint Joseph's Hospital and informed consent was obtained from each volunteer. 3D anatomical images were acquired in another group of five healthy female volunteers and one healthy male volunteer. These experiments were approved by the Sunnybrook Health Sciences Research Ethics Board and informed consent was again obtained from each volunteer.

### $T_1$ measurements

A 2D  $T_1$  map was acquired in each of five female subjects aged 22–24 on a 3 T General Electric scanner (Software Version 22.0) using a 32-channel receive-only coil for the head (MR Instruments) and a transmit body coil (GE). A multi-shot 2D echo-planar imaging (EPI) sequence located in a medial sagittal section in the brain was repeated over multiple inversion times [parameters: TE = 34.9 ms, number of EPI segments = 4, recovery time between the excitation pulse and the next inversion pulse = 9000 ms, FOV = 25 cm × 25 cm, matrix = 256 × 256, slice thickness = 1 mm, number of slices = 1, number of averages = 5, inversion times (TI) = 50, 300, 500, 800, 1000, 2000, 3000, 3500, and 4500 ms, approximate total time for mapping = 32 min]. The images were fit pixel-by-pixel to a three parameter, single-exponential  $T_1$  recovery function in Matlab (MathWorks) to produce  $T_1$  maps. A representative map depicting the locations of the ROIs used for  $T_1$  measurements is shown in Fig. 2. For measurements, ROIs were chosen representing low myelin-containing gray matter (GM) in the frontal cortex, high myelin-containing gray matter ( $GM_m$ ) in the medial portion of the primary motor cortex, and white matter (WM) in the genu of the corpus callosum. These cortical locations were chosen with reference to the appearance of myeloarchitecture in an online human brain atlas containing myelin-stained sections (<http://www.brainmuseum.org>) and data from the literature (Hopf, 1956) to encompass the range of  $T_1$  present in the human cortex.

### Statistics

Statistical analyses were performed using SPSS software (IBM SPSS Statistics Version 20.0, IBM Corp.). Data were first assessed for normality using the Shapiro–Wilk test. Levene's test of equality of error variances was then used to test the homogeneity of variances of the  $T_1$  values across tissue types. A one-way ANOVA followed by a Tukey

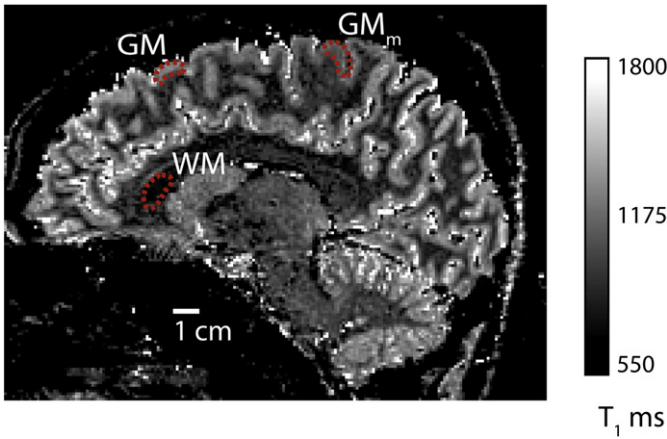


**Fig. 2.** A representative  $T_1$  map showing the locations of regions-of-interest (ROIs) for our measurements. The field-of-view of the map is cropped and low and high  $T_1$  values have been removed by thresholding during the fitting routine.

HSD post-hoc test was used to test pair-wise significant differences in  $T_1$ s between tissue types.

*Sequence optimization*

To optimize the imaging protocol, we simulated the signal,  $S_{\text{segment}}(t)$ , over the FLASH acquisition segment produced by the MP-RAGE sequence in each of three tissue types: low myelin-containing gray matter (GM), high myelin-containing gray matter ( $GM_m$ ), and white matter (WM). We modeled the signal in Matlab using published equations (Deichmann et al., 2000) (reproduced in Appendix A). The parameters used for modeling are shown in Table 1. The MP-RAGE signal depends on a given tissue's  $T_1$  and proton density ( $\rho$ ) values and we used the  $T_1$  values we measured for each tissue type in this study and  $\rho$  values from a previous study in non-human primates (Bock et al., 2009) as an estimate of  $\rho$  values in humans. We interpreted  $S_{\text{segment}}(t)$  as representing a centric-ordered k-space acquisition,  $S(t)$ , which is the signal over k-space in the phase-encoding direction of the inner loop of the MP-RAGE sequence. For segment numbers greater than one, we replicated and organized  $S_{\text{segment}}(t)$  to produce  $S(t)$ . To examine the effect of  $S(t)$  on image contrast and blurring, we calculated the point-spread-function (PSF) for each tissue type by finding the inverse Fourier transform of  $S(t)$ ,  $S(k)$ . We took the maximum magnitude amplitude of the PSF,  $A$ , as a measure of signal amplitude in a voxel for a given tissue type. We defined PSF contrast,  $\Delta A$ , as the difference between the amplitude of the PSFs for two tissue types:

$$\Delta A = |A_{\text{tissue 1}} - A_{\text{tissue 2}}|. \tag{1}$$

**Table 1**  
The parameters used for simulation of the MP-RAGE signal ( $\rho$  = relative proton density).

Tissue parameters	
$T_1$ GM	1283 ms
$T_1$ $GM_m$	1112 ms
$T_1$ WM	735 ms
$\rho$ GM	1.0
$\rho$ $GM_m$	0.97
$\rho$ WM	0.86
Pulse sequence parameters	
$N_{\text{readout}} \times N_{\text{pe1}} \times N_{\text{pe2}}$	240 × 200 × 160
$FOV_{\text{readout}} \times FOV_{\text{pe1}} \times FOV_{\text{pe2}}$	240 mm × 200 mm × 160 mm
$\tau = \text{FLASH TR} \times N_{\text{pe1}} / N_{\text{segments}}$	8.4 ms × 200 / 4 = 420 ms

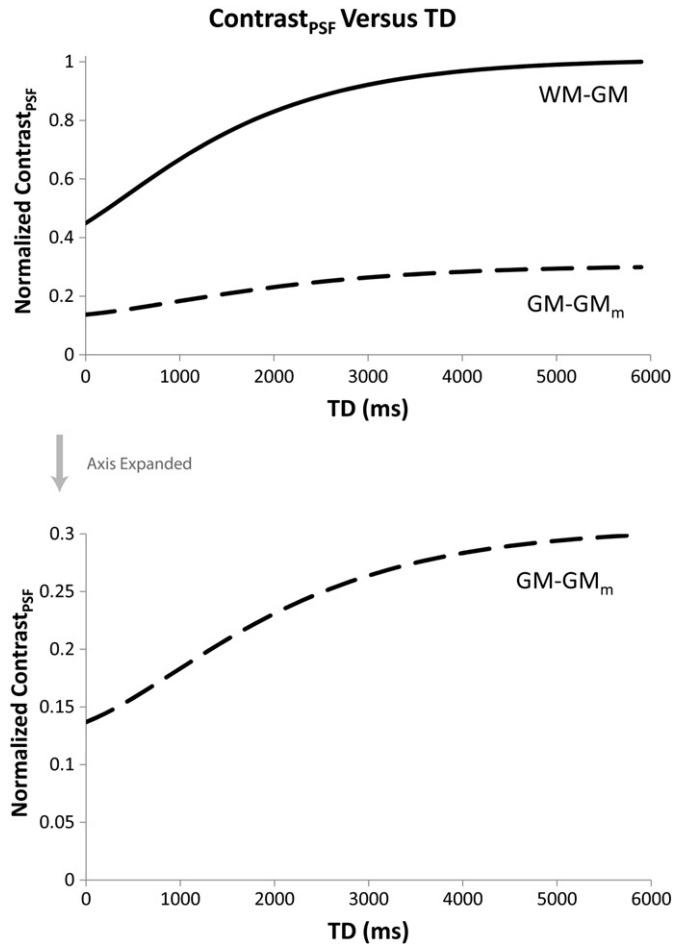


**Fig. 3.** (Top) Simulated point-spread-function contrast as a function of TD for an MP-RAGE pulse sequence calculated at a fixed TI of 1000 ms. The contrast is normalized to the maximum value for contrast between WM and GM. (Bottom) The vertical scale is expanded to better show the shape of the GM- $GM_m$  contrast curve.

Finally, we estimated image blurring by expressing the pixel value in the PSF immediately adjacent the peak pixel as a percent of the peak amplitude value (Deichmann et al., 2000).

We first demonstrated the effect of increasing the segment delay, TD, on PSF contrast in the MP-RAGE sequence. Since the noise in an MP-RAGE image is dictated by the FLASH parameters, and which remained unchanged in our simulations, the behavior of the contrast

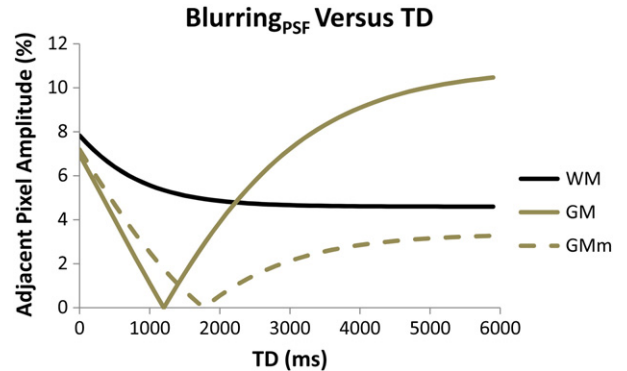


**Fig. 4.** Simulated point-spread-function blurring expressed as the percent amplitude of the pixel immediately adjacent to the peak amplitude pixel in the PSF as a function of TD for an MP-RAGE pulse sequence calculated at a fixed TI of 1000 ms.

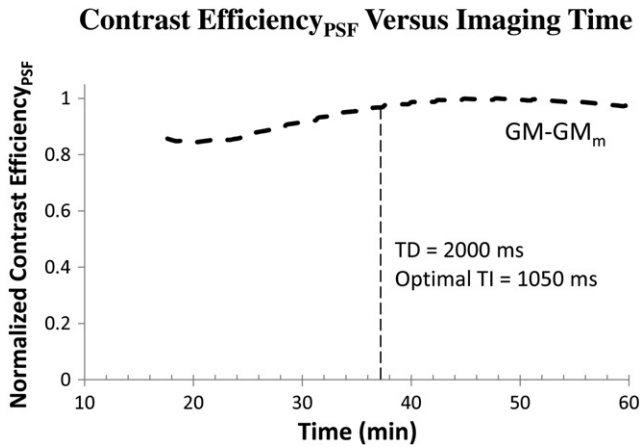


Fig. 5. Simulated point-spread-function contrast efficiency as a function of the total imaging time for the MP-RAGE pulse sequence as TD is varied from 0 to 4000 ms and the optimum TI is calculated at each TD. Contrast efficiency is normalized to its maximum value. We indicate where we imaged at TD=2000 ms (although we actually used a TI of 1000 ms for our images).

gives the entire picture of contrast-to-noise (CNR) when changing TD or TI. We varied TD over a range of 0–11,000 ms in our simulation with a fixed TI of 1000 ms, a FLASH-segment flip angle of  $12^\circ$  and with four FLASH segments (Fig. 3). The resulting plot shows that both the overall anatomical contrast (GM–WM) and the intracortical contrast (GM–GM<sub>m</sub>) rise with increasing TD, then plateau when TD is long enough that the longitudinal magnetization following the FLASH segment has relaxed to close to its equilibrium value prior to the next  $180^\circ$  inversion pulse. Thus, the overall anatomical contrast and intracortical contrast in the brain can be increased by imaging with a longer TD.

In magnetization-prepared sequences, parameters that affect contrast can also affect image blurring, which is dictated by how  $S_{\text{segment}}(t)$  evolves over the FLASH acquisition segment. Since the contrast from cortical myelin arises in deeper cortical layers, we do not consider blurring at the gray matter/CSF boundary, but only at the gray/white matter boundary and within the gray matter itself. Fig. 4 shows a plot of blurring for the given tissue types as represented by the pixel value in the PSF immediately adjacent to the peak pixel in percent of the peak amplitude value as a function of TD using the same parameters as in the contrast curve in Fig. 3. GM and GM<sub>m</sub> have minimum values for shorter TDs of roughly 1200 and 1800 ms respectively where the value of  $S_{\text{segment}}(t)$  at the beginning of the FLASH segment is close to its value at the end. The blurring in WM decreases steadily with increasing TD. There is thus a trade-off between minimizing blurring in GM and

GM<sub>m</sub> or in WM when choosing TDs for the chosen sequence parameters and so we did not optimize TD based on blurring.

To determine our optimum TD, we had to consider contrast efficiency. Changing TD affects the overall imaging time for the sequence. Moreover, an optimum TI should be calculated for each TD, which will also affect image time. We thus examined the PSF contrast efficiency when increasing TD, defined as:

$$\text{ContrastEfficiency} = \frac{\Delta A}{\sqrt{t}} \quad (2)$$

where  $t$  is the total imaging time of the sequence. Fig. 5 plots the intracortical contrast (GM–GM<sub>m</sub>) efficiency against the total imaging time as TD is varied from 0 to 4000 ms for a flip angle of  $12^\circ$  and four FLASH segments. The optimum TI is found for each TD by calculating PSF contrast over a range of TI from 0 to 2000 ms and choosing the TI which produces the maximum value of contrast. Where the slope of the contrast efficiency curve is positive, the effect of lengthening TD is better than image averaging for producing CNR. We chose a TD of 2000 ms where the contrast efficiency was still improving, but the imaging time wasn't excessively long. Fig. 6 left shows a plot of contrast versus TI for a TD of 2000 ms at a flip angle of  $12^\circ$  and with four segments. The maximum GM–GM<sub>m</sub> contrast occurs around a TI of 1050 ms and we chose a TI value of 1000 ms for imaging. The curve for intracortical contrast is quite broad and changes by less than 3% over a range of 875–1275 ms, so our TI choice still produces a near maximum GM–GM<sub>m</sub> contrast. In addition, since the contrast curve is broad, it is unlikely that TI needs to be optimized on a per subject basis as long as subjects have the same age and health status. In Fig. 6 right, we show the effects of blurring from the simulation. The GM<sub>m</sub> blurring is near its minimum at the chosen TI, and the WM and GM blurring are approximately equal.

Next, we simulated the effect of flip angle on image contrast. Fig. 7 left shows the point-spread function contrast as a function of flip angle for TD=2000 ms, TI=1000 ms, and four segments. In Fig. 7 right, we plot the blurring as a function of flip angle. In the first curve, the contrast increases as the flip angle increases to a maximum at a flip angle of  $14^\circ$ , after which the additional contrast provided by the increasing flip angle is offset by rapid signal decay over the FLASH segment. We chose a flip angle of  $12^\circ$  to produce a near maximum GM–GM<sub>m</sub> contrast while attempting to minimize the blurring of WM voxels which can make segmentation difficult.

Finally, we examined the effect of the number of FLASH segments on image contrast and contrast efficiency. In Fig. 8 left, we plot PSF contrast as a function of the number of segments for TD=2000 ms, TI=1000 ms, and flip angle =  $12^\circ$ . Fig. 8 right plots blurring as a function of the number of segments. The contrast curve demonstrates that increasing the number of segments produces better contrast as the length of the FLASH segment is shortened and there is thus less signal evolution over k-space. Fig. 8 right shows that blurring is little changed by

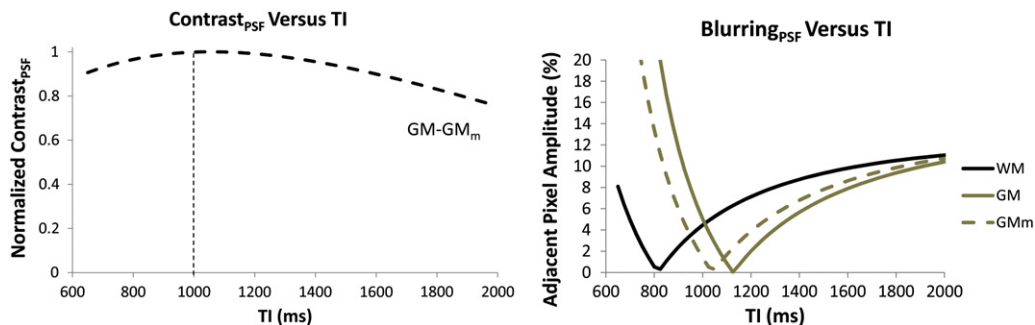


Fig. 6. (Left) Simulated point-spread-function contrast as a function of TI for a fixed TD of 2000 ms. Contrast is normalized to its maximum GM–WM value. We indicate where we imaged at TI=1000 ms. (Right) Simulated point-spread-function blurring as a function of TI.

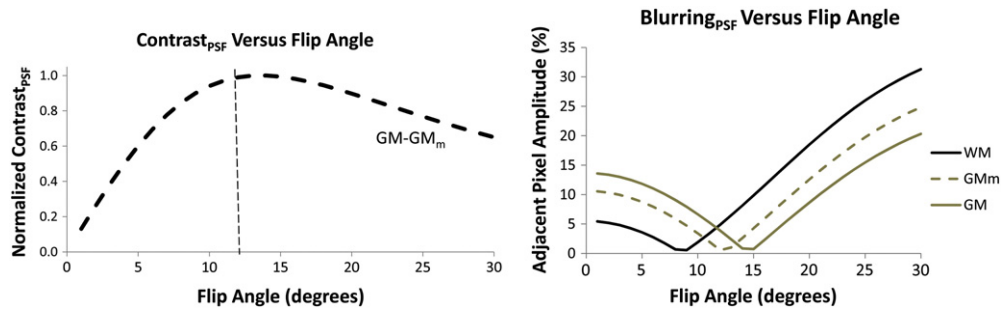


Fig. 7. (Left) Simulated point-spread-function contrast as a function of flip angle. We indicate the flip angle of 12° used for imaging. (Right) Simulated point-spread-function blurring as a function of the flip angle.

increasing the number of segments. We thus chose four segments for imaging. With final optimum parameters, the blurring was 5% in WM, 4% in GM, and 0.5% in GM<sub>m</sub>.

Increasing the number of segments also increases the imaging time, however, so we considered the PSF contrast efficiency versus the number of segments, plotted in Fig. 9.

In this case, the slope of the curve is slightly positive between one and two segments, and decreases slightly thereafter. This indicates that increasing the number of segments and image averaging actually have a similar effect on improving CNR.

### 3D anatomical imaging at 1 mm isotropic resolution

Sets of whole-brain 3D anatomical images were acquired in each of five female subjects aged 21–30 and one male aged 29 years on a Philips Achieva 3 T MRI scanner (software version 3.2.1) using a Philips 8 channel receive-only radiofrequency (RF) head coil and a Philips body coil for transmission. A whole-brain slab-selective 3D MP-RAGE sequence was collected for image segmentation purposes (see “Standard MP-RAGE (1 mm)” entry in Table 2 for specific parameters). The sequence used an adiabatic inversion pulse, had an isotropic resolution of 1 mm, a single average, and took 7:25 min to acquire.

Another slab-selective 3D MP-RAGE sequence optimized to produce intracortical T<sub>1</sub> contrast was collected to visualize cortical myelination (“High contrast MP-RAGE (1 mm)” in Table 2). The sequence used an adiabatic inversion pulse, had an isotropic resolution of 1 mm, a single average, and took 36:29 min to acquire. In one subject, the same sequence was repeated with a reduced TD for contrast comparison [parameters: TD = 500 ms, imaging time = 20:29 min].

A final slab-selective proton density-weighted 3D FLASH sequence was collected to correct some of the B<sub>1</sub> bias field effects in the MP-RAGE images (“FLASH (1 mm)” in Table 2). The sequence had an isotropic resolution of 1 mm, was averaged two times and took 8:57 min to acquire.

### 3D anatomical imaging at 0.5 mm isotropic resolution

A pair of 3D anatomical images was acquired, covering the occipital cortex in one 29 year-old male subject using a 5 inch diameter surface coil (Philips) placed over the occipital pole. Imaging was performed using the high contrast MP-RAGE sequence (“High contrast MP-RAGE (0.5 mm)” in Table 2) optimized for the increased resolution and a 3D FLASH sequence (“FLASH (0.5 mm)” in Table 2). Both sequences had an isotropic resolution of 0.5 mm. The MP-RAGE sequence had a single average and took 29:38 min to acquire, while the FLASH sequence was averaged two times and took 11:17 min to acquire.

### Post-processing at 1 mm isotropic resolution

For each individual, the 3D high contrast MP-RAGE image was placed into a standard Talairach coordinate system with the anterior and posterior commissures lying in a common axial plane using a rigid transformation in Amira (Visage Imaging). The 3D standard MP-RAGE and 3D FLASH images were rigidly registered to this image so that all images were in a common space. After calculating the necessary transformation, each image was resampled to the common space using a single Lanczos interpolation. The FLASH image was filtered with a 3D median filter of 5 × 5 × 5 kernel size to reduce noise. The high contrast MP-RAGE image

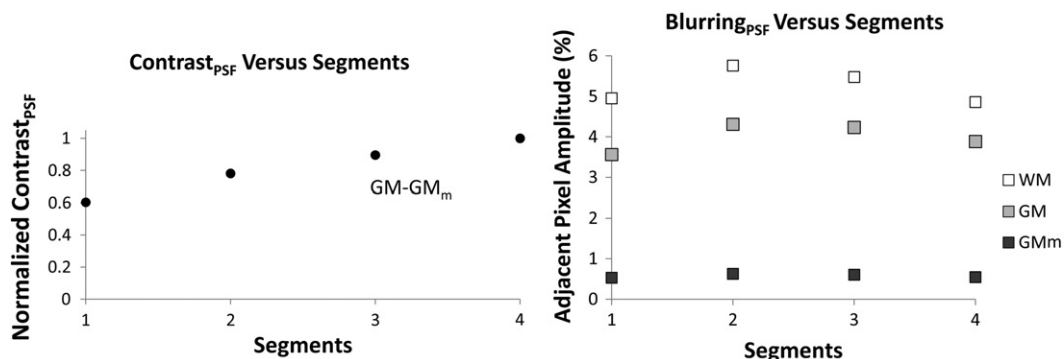


Fig. 8. (Left) Simulated point-spread-function contrast as a function of the number of FLASH segments in the MP-RAGE. We indicate the four segments used for imaging. Contrast is normalized to its maximum value. (Right) Simulated point-spread-function blurring as a function of the number of FLASH segments.

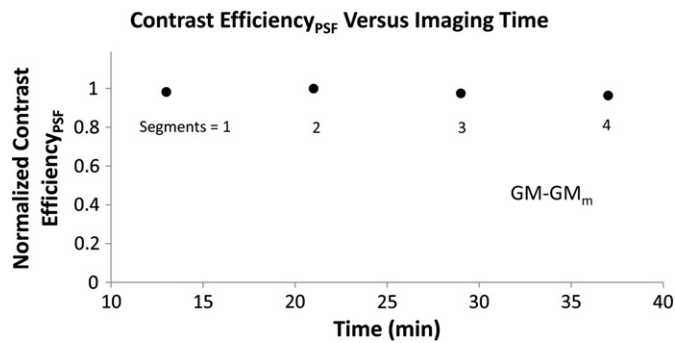


Fig. 9. Simulated point-spread-function contrast efficiency as a function of the total imaging time as the number of FLASH segments is increased. Contrast efficiency is normalized to its maximum value.

was then divided by the FLASH image to produce a new ratio image to remove the effects of the  $B_1^-$  bias field representing the sensitivity of the receiver coil and partially remove the effect of the  $B_1^+$  bias field representing the sensitivity of the transmitter coil (Marques et al., 2010; Van de Moortele et al., 2009; Wang et al., 2005). The 3D standard MP-RAGE image was automatically segmented in FreeSurfer (<http://surfer.nmr.mgh.harvard.edu/>) to extract a rough white matter mask. The mask was then used to guide fine white matter segmentation in the ratio image, based on intensity thresholding in Amira. A surface mesh was created from the fine white matter segmentation and the resulting surface was outwardly displaced along its normals. This created a new surface at a depth that is roughly 25% of the distance between the white matter and pial surface in the myelinated lower layers of the cortex, confirmed by manual inspection. For display purposes, the nearest-neighbor MRI intensity data from the ratio image at the depth of this surface was displayed on it with an orange colormap. Neither the intensity data nor the surface data were smoothed in any operations to preserve fine details in the resulting images.

#### Post-processing at 0.5 mm isotropic resolution

The processing of the 0.5 mm isotropic images was identical to the processing described for the 1 mm isotropic images except that the initial rough white matter mask was created manually in the ratio image rather than automatically from a standard anatomical image in FreeSurfer, as in the 1 mm case.

#### Surface inflation

The cortical surface with the intensity data displayed in one subject at 1 mm isotropic resolution was inflated in Caret (Van Essen et al., 2001; [www.nitrc.org/projects/caret/](http://www.nitrc.org/projects/caret/)) to show the pattern of

myelin density within the cortical folds. The cortical surface was inflated using 1500 iterations with smoothing every 10 iterations and an inflation factor of 1.02.

## Results

### $T_1$ Measurements

The results of the  $T_1$  measurements are shown in Table 3. We measured WM  $T_1$  to be  $735 \pm 30$  ms, which is in good agreement with measured values from other studies at 3 T also in the genu of the corpus callosum of 721 ms (Lu et al., 2005) and 724 ms (Zhu and Penn, 2005). We measured GM  $T_1$  to be  $1283 \pm 23$  ms, which is in the range of measured values from other studies in frontal gray matter of 1209 ms (Lu et al., 2005) and 1322 ms (Wansapura et al., 1999). Finally,  $GM_m T_1$  was  $1112 \pm 44$  ms. Across subjects, there was thus a decrease in  $T_1$  of  $171 \pm 40$  ms (mean  $\pm$  standard deviation of the paired differences,  $n=5$ ) between GM and  $GM_m$  and  $548 \pm 47$  ms between GM and WM. Typically, anatomical imaging is optimized on the basis of the 548 ms  $T_1$  difference between gray matter and white matter to visualize gross anatomy in the brain; we sought to optimize the sequence, however, to exploit the smaller 171 ms difference and produce intracortical contrast. It should be noted that the  $T_1$ s we measured were suitable for optimizing the imaging of the subjects in this study, but that  $T_1$ s should be measured again in future studies featuring subjects of different age or health status, or imaging performed at other field strengths.

### Sequence optimization

To confirm the main simulation finding that intracortical contrast can be better increased by lengthening TD versus image averaging, we made two whole-brain images with the MP-RAGE sequence at 1 mm isotropic resolution with a TD of 500 ms or 2000 ms. Fig. 10 shows a sagittal slice from each image. We measured the GM- $GM_m$  signal difference,  $\Delta S$ , in the MP-RAGE images as the absolute mean signal difference between ROIs placed in GM and  $GM_m$  respectively.  $\Delta S$  is analogous to  $\Delta A$  from our simulations. We then divided  $\Delta S$  by the standard deviation of the noise in the image background to yield  $\Delta SNR$ . Dividing  $\Delta SNR$  by the imaging time yielded  $\Delta SNR$  efficiency. The GM- $GM_m$   $\Delta SNR$  efficiency was 6.8 in the TD = 2000 ms image versus 5.7 in the TD = 500 ms scan, showing that increasing TD in fact improves  $\Delta SNR$  efficiency. The bottom panel of Fig. 10 shows the final surface processed data from the TD = 500 ms and TD = 2000 ms images, which shows that the increased  $\Delta SNR$  is necessary to better resolve intracortical features.

We also show in Fig. 10 a slice from the proton-density weighted FLASH sequence by which we divide our MP-RAGE to correct some image intensity inhomogeneities. Correcting  $B_1^-$  and  $B_1^+$  bias fields is important for imaging cortical myelination because the resulting

Table 2

Pulse sequence parameters from Methods. Matrix and FOV are given as readout  $\times$  phase encode (FLASH inner loop)  $\times$  phase encode (slab-selective outer loop).

Sequence	Matrix	FOV (mm)	TI (ms)	TD (ms)	Flip angle (degrees)	TE (ms)	TR (FLASH) (ms)	FLASH segments
Standard MP-RAGE (1 mm)	240 $\times$ 200 $\times$ 160	240 $\times$ 200 $\times$ 160	1100	0	7	3.8	8.4	1
High contrast MP-RAGE (1 mm)	240 $\times$ 200 $\times$ 160	240 $\times$ 200 $\times$ 160	1000	2000	12	3.8	8.4	4
FLASH (1 mm)	240 $\times$ 200 $\times$ 160	240 $\times$ 200 $\times$ 160	–	–	4	3.8	8.4	–
High contrast MP-RAGE (0.5 mm)	336 $\times$ 336 $\times$ 120	168 $\times$ 168 $\times$ 60	1000	2000	12	3.8	8.4	4
FLASH (0.5 mm)	336 $\times$ 336 $\times$ 120	168 $\times$ 168 $\times$ 60	–	–	4	3.8	8.4	–

**Table 3**

$T_1$  measurements at 3 T in the brains of healthy female subjects aged 22–24. Values are given as mean  $\pm$  standard deviation ( $n=5$ ). All possible pairwise comparisons are statistically significant at the  $p<0.05$  level (key: GM = low myelin containing gray matter,  $GM_m$  = high myelin containing gray matter, WM = white matter).

Tissue	$T_1$ (ms)
GM	1283 $\pm$ 23
$GM_m$	1112 $\pm$ 44
WM	735 $\pm$ 30

intensity variations can easily overwhelm the subtle intracortical intensity variations related to the myelin content of the cortex. The signal in the MP-RAGE image,  $S_M$ , can be expressed as:

$$S_M \propto M_M |B_1^-| \sin(\alpha |B_1^+|) e^{-\frac{TE}{T_1}} \quad (3)$$

where  $M_M$  is the spatially varying longitudinal magnetization produced by the MP-RAGE sequence,  $B_1^-$  represents the spatially varying scalar sensitivity profile arising from the RF receiver coils,  $\alpha$  is the prescribed flip angle,  $B_1^+$  is the spatially varying scalar sensitivity

profile arising from the RF transmitter coil, TE is the echo time, and  $T_2^*$  is effective transverse relaxation time. Similarly, the signal in the FLASH image,  $S_F$ , can be expressed as:

$$S_F \propto M_F |B_1^-| \sin(\beta |B_1^+|) e^{-\frac{TE}{T_2^*}} \quad (4)$$

where  $\beta$  is the prescribed flip angle. Since both images are made with the same RF transmitter and receiver coils and with the same TE, the signal in the ratio image,  $S_R$ , is given by:

$$S_R \propto \frac{S_M}{S_F} \propto \frac{M_M \sin(\alpha |B_1^+|)}{M_F \sin(\beta |B_1^+|)} \quad (5)$$

For small values of  $\alpha$  and  $\beta$ , Eq. (6) can be approximated as:

$$S_R \propto \frac{M_M \alpha}{M_F \beta} \quad (6)$$

This shows that the effects of the  $B_1^-$  bias field are removed in the ratio image, and some effects of the  $B_1^+$  field are removed, as well

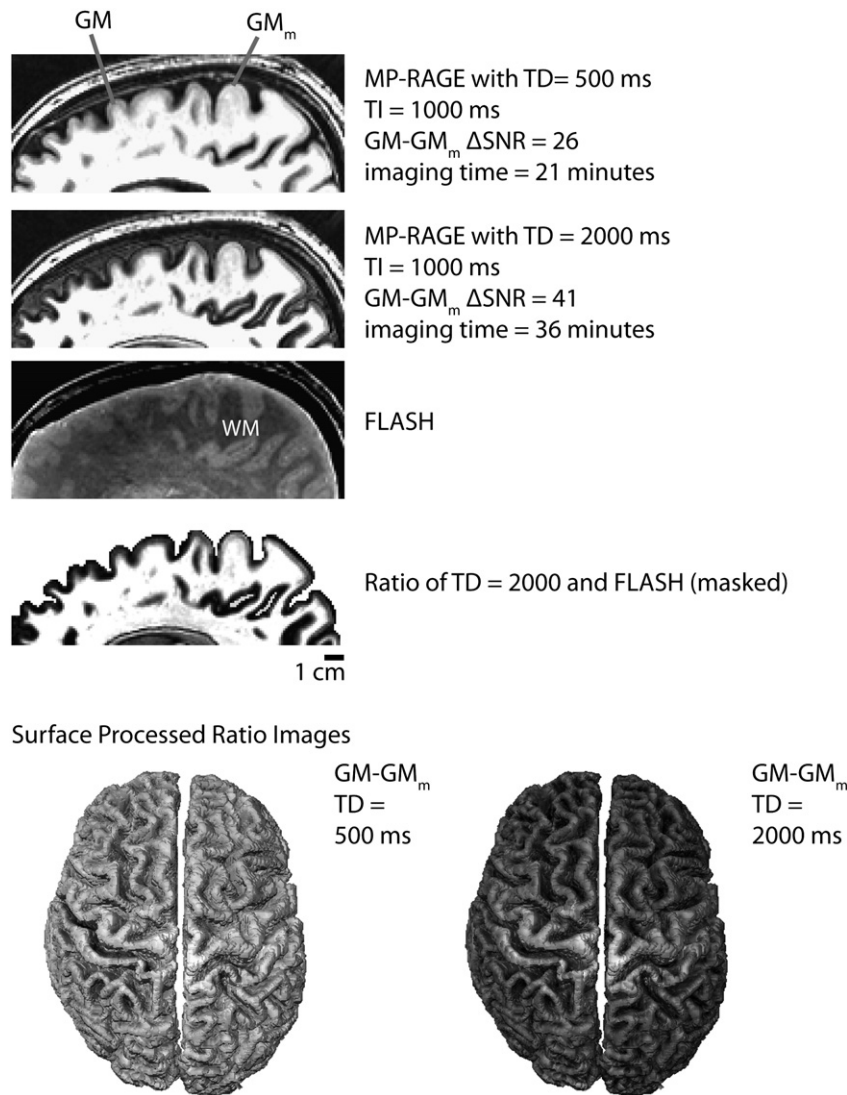


**Fig. 10.** Cropped sagittal slices from 3D images made at 1 mm isotropic resolution in the same subject using the MP-RAGE sequence with two different TDs and the FLASH sequence. All three images are displayed using the same window and leveling. The ratio image is formed by dividing MP-RAGE image at TD = 2000 ms by a median-filtered version of the FLASH image. The ratio image is masked to show only the cortex and white matter. The bottom of the figure shows processed images of the cortical surface made with the TD = 500 ms and TD = 2000 ms display at the same window and level.

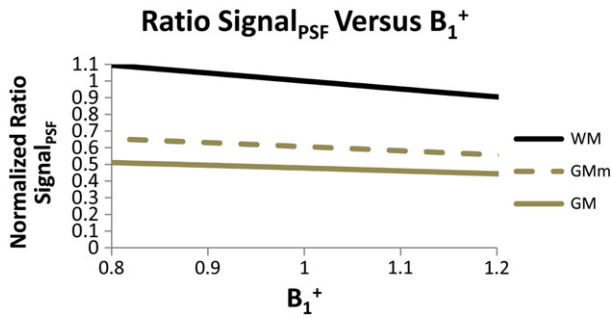


**Fig. 11.** Simulated point-spread-function ratio signal in three tissue types as a function of  $B_1^+$  where the actual flip angle, FA, is given by prescribed flip angles,  $\alpha$  or  $\beta$ , multiplied by  $B_1^+$ . The ratio signal is normalized to its value for  $B_1^+ = 1$  in WM. This corresponds to the correct prescribed angle.

(Marques et al., 2010). However,  $M_M$  and  $M_F$  are still a function of  $B_1^+$  so that:

$$S_R \propto \frac{M_M(\alpha|B_1^+)|\alpha}{M_F(\beta|B_1^+)|\beta}. \quad (7)$$

To estimate the effect of the residual  $B_1^+$  bias field in our ratio image, we simulated Eq. (7) for our MP-RAGE sequence ( $\alpha = 12^\circ$ ) and for our FLASH sequence ( $\beta = 4^\circ$ ) while varying  $B_1^+$  for the three tissue types (plotted in Fig. 11). This shows that for a maximum  $B_1^+$  variation between 0.9 and 1.1 (20%), the PSF ratio signal in GM and

in  $GM_m$  would vary by about 8%. In a  $B_1^+$  map we made in one individual using a variable TR mapping method (Voigt et al., 2010), we noted a maximum variation in  $B_1^+$  of about 20% (mean  $0.95 \pm$  standard deviation 0.05). This map was smoothly varying over the entire cortex, but according to our estimation, could produce signal differences in distant areas of the cortex of up to 8%.

In our FLASH sequence, we use a low flip angle so the image is mostly proton-density weighted and contains as little  $T_1$ -weighting as possible, which would reduce the contrast in the MP-RAGE image following the division. There is still proton-density contrast between gray matter and white matter, which reinforces the contrast in the MP-RAGE image during the division. There is no visible contrast within the cortex, however, presumably because the presence of cortical myelin has little effect on proton density values in tissue. Thus, the intracortical contrast in the ratio image still reflects the  $T_1$ -weighted contrast of the MP-RAGE. One could also combine the MP-RAGE and FLASH images in the same pulse sequence, as done in MP-2RAGE (Marques et al., 2010), and then increase the delay time between the second FLASH segment in that sequence and the next  $180^\circ$  pulse to produce the same contrast as our optimized MP-RAGE.

Next, we used the MP-RAGE sequence with a  $TD = 2000$  ms to make 1 mm isotropic images over the whole cortex in five female subjects. Our final surface-rendered images are shown in Figs. 12 (top) and 14. In Fig. 12, there is an expected increase in signal intensity associated with increased myelin in the pre-central gyrus corresponding to the location of M1 (Geyer et al., 2011; Glasser and Van Essen, 2011; Hopf, 1956), in the post-central gyrus corresponding to the location of S1 (Glasser and Van Essen, 2011; Hopf, 1970; Hopf and Vitzthum, 1957),

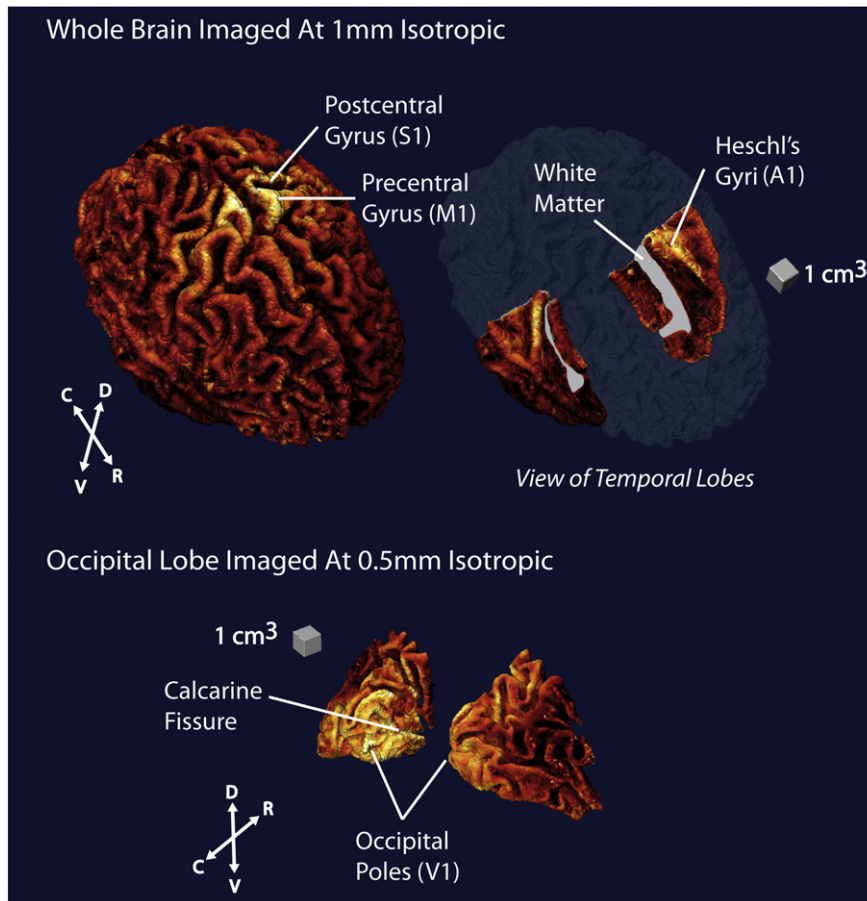


**Fig. 12.** (Top) Isometric views of surface-rendered MRI data from a 3D high contrast MP-RAGE image with 1 mm isotropic resolution displayed by an orange colormap to highlight contrast. The cortical regions associated with the major signal enhancements are labeled (S1 = primary somatosensory cortex, M1 = primary motor cortex, A1 = primary auditory cortex, c = caudal, r = rostral, v = ventral, d = dorsal). (Bottom) Caudal view of surface-rendered data from the same sequence with a 0.5 mm isotropic resolution collected in a different subject (V1 = primary visual cortex).

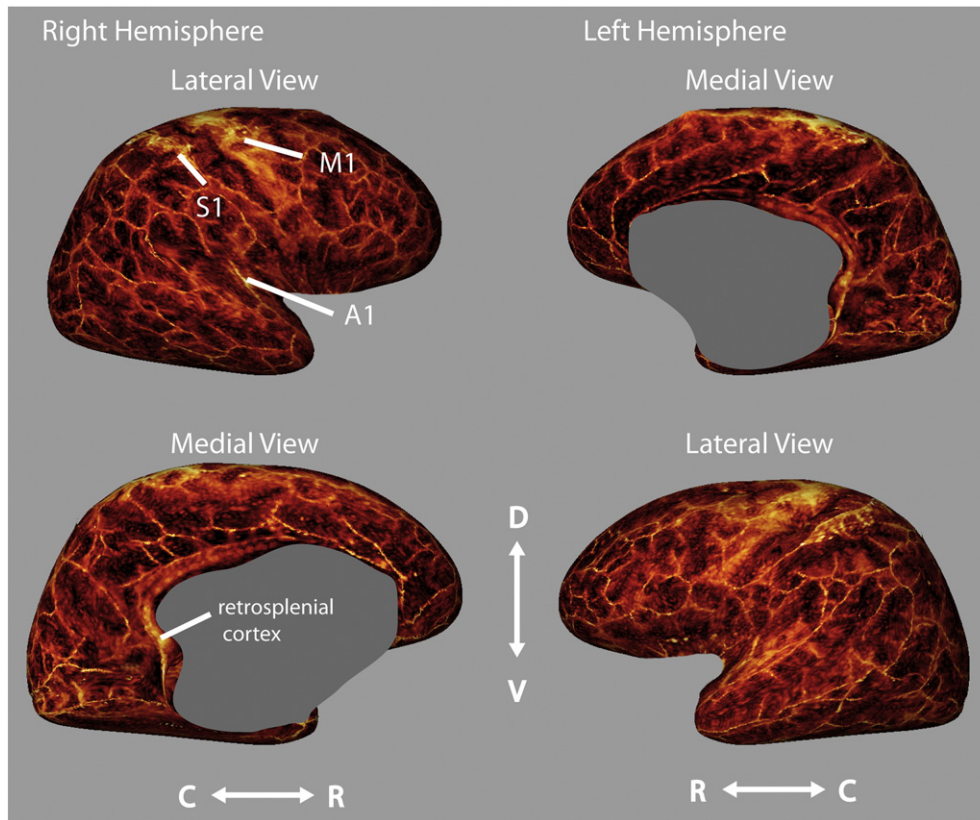


Fig. 13. Views of the flattened cortical surface of an individual imaged at 1 mm isotropic resolution.

and in Heschl's gyri corresponding to the location of A1 (Hopf, 1955, 1968; Sigalovsky et al., 2006).

Fig. 13 shows the surface of the cortex imaged at 1 mm isotropic resolution in an inflated presentation to visualize the enhancement pattern within the sulci. This view also shows strong image enhancement in the retrosplenial cortex. There are lines of increased enhancement that correlate with the location of the gyri, and areas of decreased enhancement that correlate with the location of sulci. These features may reflect partial volume effects in our relatively low resolution 1 mm isotropic images that lead to problems accurately defining the surface in the sulcal depths or on the crowns of gyri.

The cortical myelin density pattern was best reproduced over all four subjects in M1 (Fig. 14), which is unsurprising for this is the region of the human cortex with the thickest myelinated layers, at 2.2 mm (Zilles et al., 2012). The pattern over A1, whose myelinated layers are of 1.6 mm thickness (Zilles et al., 2012), showed greater variation, although this may be caused by a high morphological variability in that region, as has been noted in other studies (Sigalovsky et al., 2006). We also observed some enhancement in S1, where the myelinated layers are only of 0.9 mm thickness (Zilles et al., 2012), in all individuals, although the enhancement pattern was less reproducible. At 1 mm isotropic resolution, however, we did not see a reproducible increase in signal intensity in the location of the medial occipital lobe and calcarine fissure associated with V1, whose myelinated layers are of 1.1 mm thickness (Zilles et al., 2012). That resulted from an inability to identify the gray/white matter boundary because of a partial volume effect between the white matter and the highly convoluted, thin cortex. The partial volume effect was lower in S1 because this cortical region is less convoluted than V1. The problem was resolved by imaging at 0.5 mm resolution, resulting in a better definition of the white matter boundary and visualization of the stripe of Gennari (Fig. 15) and a good visualization of V1 in the surface-rendered image (Fig. 12, bottom). The loss of CNR caused by

halving the voxel dimensions in each direction was recovered by using a localized surface coil to image only the occipital cortex.

## Discussion

Our results demonstrate that intracortical contrast can be improved by optimizing a  $T_1$ -weighted pulse sequence beyond the usual optimizations performed to produce gross anatomical contrast in the brain. With the optimized sequence, known highly myelinated cortical regions can be identified in individual subjects at 3 T using optimized  $T_1$ -weighted imaging. Thicker regions, such as M1 and A1 can be resolved in whole-cortex images with an isotropic resolution of 1 mm while thinner regions like V1 can be resolved in targeted imaging with an isotropic resolution of 0.5 mm.

There is still room for improvement in the technique to produce robust maps of cortical myelin content in individuals. Owing to the thinness of myelinated cortex, it would be ideal to increase the imaging resolution to improve the visualization of patterns of cortical myelin content in all regions, even thick ones. The increase in resolution would reduce partial volume effects between white matter and the myelinated lower gray matter layers and would likely improve segmentation and definition of the surface through the lower cortical depths. This was illustrated when imaging the occipital cortex in one individual at 0.5 mm isotropic resolution. Increasing the resolution would require a larger image matrix size, which would increase imaging time even further than the long times already needed unless CNR can be improved. It is likely that we are close to the resolution limit in our  $T_1$ -weighted 3D images of the whole cortex at 1 mm isotropic resolution. The use of parallel imaging techniques with acceleration factors greater than 1 would speed the imaging, but at the expense of CNR, which is already limited in our technique. Some CNR may be gained using other contrast

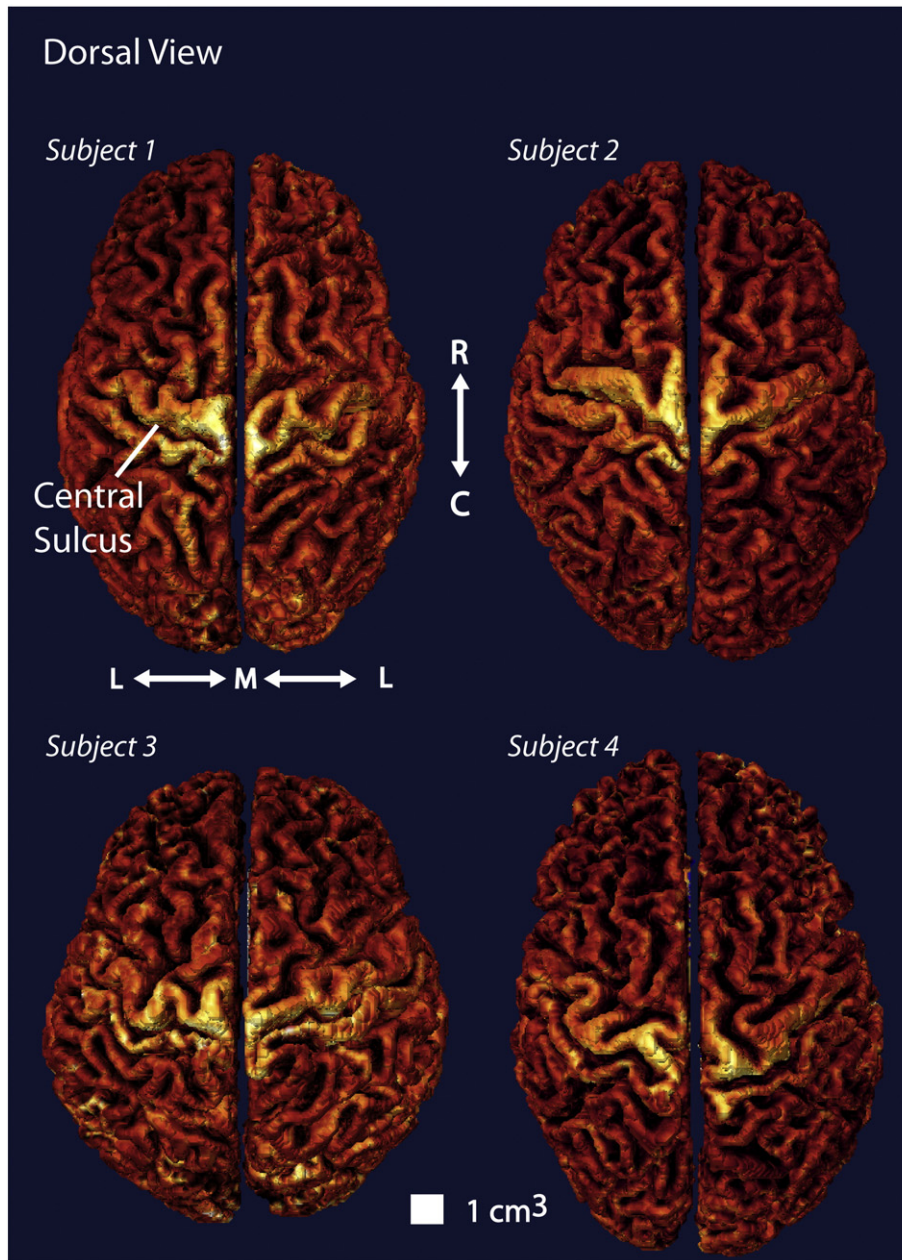


**Fig. 14.** Surface-rendered MRI data from 3D MP-RAGE images at 1 mm isotropic resolution in four healthy female subjects showing reproducibility in the appearance of M1, a major feature of the myeloarchitecture (L = lateral, M = medial).

mechanisms that have proved reliable for generating myelin-related contrast such as  $T_2$ ,  $T_2^*$ , magnetization transfer (MT), or diffusion.

Likely the best way to image the entire cortex at a sub-millimeter isotropic resolution in individuals in a single scan is to move to higher field strength. This has initially been demonstrated at 7 T, where greater signal from each tissue type results in higher CNR between tissues (Weiss et al., 2010). The TD in the MP-RAGE sequence could then be reduced to shorten the imaging time if a higher resolution was needed, while preserving the CNR of the resulting image. This approach relies on the fact that the differences in MR parameters between areas of the cortex with low and high myelin contents are preserved as one moves to higher fields. In a previous study of monkeys at 7 T (Bock et al., 2009), we measured a  $T_1$  difference of 270 ms over the cortex, which bodes well for imaging myeloarchitecture at 7 T in individual humans by  $T_1$ -weighted imaging. Steps will need to be taken at higher field strengths, however, to diminish the increased effects of the  $B_1^+$  bias field.

In imaging at 3 T, one way to increase CNR during the post-processing of the images would be to divide the MP-RAGE image with an image with the inverse intracortical contrast (Glasser and Van Essen, 2011), rather than the proton-density FLASH image which has little if any intracortical contrast.  $T_2$  and  $T_2^*$ -weighted sequences both produce images where the signal intensity is lower in regions with a high myelin content and could be used for the division, although  $T_2^*$  may not be a good choice because the contrast is orientation dependent.  $T_2$ -weighting can be obtained using a spin-echo based sequence, although this sequence will have lower spatial distortion than our gradient echo-based MP-RAGE sequence. Thus the images may need to be accurately and non-linearly registered (Woods et al., 1999) to the MP-RAGE image prior to the division. If this registration performed well and per-voxel correspondence could be achieved between the images, it would be a viable way to increase contrast in the final ratio image while still preserving fine spatial detail.

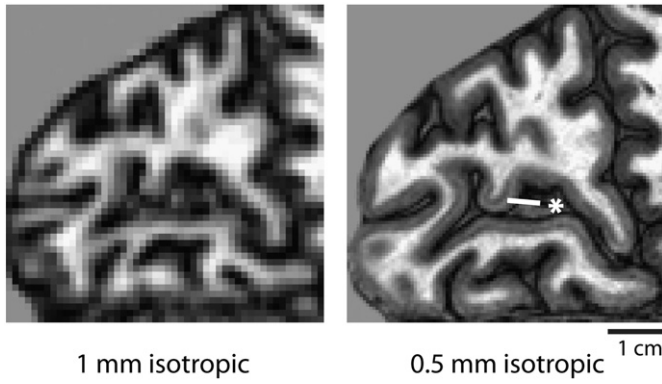


**Fig. 15.** Cropped sagittal slices from 3D MP-RAGE images collected at 1 mm and 0.5 mm isotropic resolution respectively in the same subject showing the better definition of the gray/white matter boundary for segmentation in the higher resolution image. The images have been masked to show only gray/white matter voxels. The asterisk identifies the stripe of Gennari, a structure that defines the extent of V1 accurately if it can be resolved.

Beyond increasing resolution in an image of the whole cortex, higher resolutions at 3 T can be achieved using targeted imaging of specific cortical regions, as we showed in imaging of the occipital cortex. There, the expected decrease in CNR caused by halving the voxel size in each direction was recovered using a single loop surface coil appropriately sized for the occipital cortex. It is likely that larger gains in CNR could be realized with parallel array coils designed specifically to image specific regions of the cortex – similar coil optimizations are commonly used in fMRI studies of specific areas such as V1 (Barth and Norris, 2007). This is probably the most viable approach to study myeloarchitecture at 3 T in individuals, for our whole-cortex imaging at 1 mm isotropic resolution could not resolve all of the major myelinated cortical regions accurately. One could easily target M1, A1, and S1 with a single high resolution image, since these regions are relatively close to each other, and then use another image for V1.

A remaining concern with our imaging technique is the long time needed to generate good intracortical CNR; the 1 mm isotropic scans took more than 36 min to acquire, which may be too long for some applications and can accumulate motion blurring if the subjects cannot remain still. One way to reduce the effects of motion blurring would be to shorten the sequence without shortening TD or TI, and recover the CNR by image averaging coupled with image registration-based motion correction. We found that segmenting the FLASH acquisition and sequence averaging had the same efficiency at producing CNR. We could have thus imaged using only one FLASH segment, which would have shortened our scans by a factor of 4, then recovered CNR by averaging the scan 4 times with motion correction applied between scans. The same approach could also be used with parallel imaging to reduce the scan time, with image averaging then applied to recover CNR.

Another outstanding issue in our technique is the influence of the residual non-uniform  $B_1^+$  bias field on our ratio image. We estimated that this would cause a worst-case signal deviation of 8% in GM and  $GM_m$  voxels in our images. Although  $B_1^+$  was smoothly varying over our image, and the features we identified relied mainly on local contrast to be resolved, care should be taken in interpreting signals across the entire cortex (for example, comparing image intensity in lateral portions of M1 between hemispheres). One approach to lessen the effect of the residual  $B_1^+$  bias field is to use parallel transmission to improve its homogeneity (Katscher and Börner, 2006). Concurrently, methods for correcting the effects of  $B_1^+$  bias fields on the magnetization of MP-RAGE and FLASH sequences should also be explored, although this may be intractable as it would require knowledge of the  $T_1$  and proton density values of each voxel. For instance, one can see in Fig. 11 that the effect of  $B_1^+$  variation on signal is different for each of the three brain tissue types investigated.

Finally, to improve visualization of the pattern of myelin content over the cortical surface, and reduce artifacts, the surface rendering

could also be improved. Our technique is relatively simple because we can readily identify and automatically segment the gray/white matter boundary in our images using rough segmentation intensity thresholding to create a white matter surface that we then grow slightly into the deepest myelinated layers of the cortex. A more accurate method might be to also find the gray matter/CSF boundary to segment the pial surface, and then compute a new surface at a distance between it and the white matter surface at a depth that accurately samples myelination in all regions. This would move the surface for display away from encroaching white matter voxels in thick cortical regions to improve the contrast in the resulting image of the myeloarchitecture, and avoid overshooting myelinated cortex in thinner regions.

From a neurobiological standpoint, our imaging method supports ongoing developments in the creation of in vivo microanatomical native maps of the entire cortex of specific individuals. This is crucial for unraveling the overall relationship between microstructure and function in the human brain. Previously, such investigations have been limited to studies in individuals of isolated regions such as V1 (Barbier et al., 2002; Clare and Bridge, 2005; Clark et al., 1992; Sánchez-Panchuelo et al., 2012; Walters et al., 2003), A1 (Sigalovsky et al., 2006), or M1 (Kim et al., 2009) and group studies of the entire cortex (Cohen-Adad et al., 2012; Glasser and Van Essen, 2011). Studies from the pioneers of cytoarchitecture (Korbinian Brodmann) and myeloarchitecture (Cécile and Oskar Vogt) in the first half of the 20th century showed that there is a great degree of concordance between cyto- and myeloarchitectonic parcellations in the cortex and that cytoarchitectonic borders can easily be replicated in adjacent histological sections stained for myelin sheaths and vice versa (Brodmann, 1909; Vogt and Vogt, 1919). This means that myeloarchitectonic information provided by MRI in vivo likely also reflects the underlying cytoarchitecture (as in the still widely-used brain map of Brodmann). When these in vivo microanatomical maps from individuals have been combined with matched individual functional imaging data, as in the work on V1 (Bridge et al., 2005; Sánchez-Panchuelo et al., 2012), it has been possible to make direct correlations between microstructure and function in living human brains. With optimizations like ours for imaging cortical myelin content it will be possible to investigate these correlations across the entire cortex.

## Appendix A

We modeled our signal from a published equation of the MP-RAGE sequence. This is provided for completeness – please see the original paper for the derivation (Deichmann et al., 2000).

The MP-RAGE magnetization,  $M$ , for a given tissue at steady-state at the first echo in the FLASH segment is given by:

$$M = M_0 \frac{(1 - EI) - EI \cdot (1 - ED) - ED \cdot EI \cdot \frac{1 - ETR}{1 - ETR^*} \cdot (1 - E\tau^*)}{1 + ED \cdot EI \cdot E\tau^*}$$

where

$$EI = e^{-\frac{TI}{T_1}},$$

$$ED = e^{-\frac{TD}{T_1}},$$

$$ETR = e^{-\frac{TR}{T_1}},$$

$$ETR^* = e^{-\frac{TR}{T_1^*}},$$

$$E\tau^* = e^{-\frac{\tau}{T_1^*}},$$

$$\tau = \frac{N_{pe} \cdot TR}{N_{segments}},$$

$$T_1^* = \frac{T_1 \cdot TR}{TR - T_1 \cdot \ln(\cos \alpha)}$$

and  $\alpha$  = tip angle of FLASH sequence,  $M_0$  = equilibrium longitudinal magnetization in the tissue (proportional to proton density,  $\rho$ ),  $TI$  = inversion time,  $T_1$  = longitudinal relaxation time,  $TD$  = delay between the end of the FLASH segment and the next  $180^\circ$  pulse,  $TR$  = repetition time of the FLASH sequence,  $\tau$  = length of the FLASH segment,  $N_{pe}$  = number of phase encodes in the FLASH segment loop, and  $N_{segment}$  is the number of FLASH segments. The signal over the duration of the FLASH segment,  $S_{segment}$ , can be found from:

$$S_{segment}(t) = M_{segment}(t) \sin \alpha$$

where:

$$M_{segment}(t) = M_0^* \left( 1 - e^{-\frac{t}{T_1^*}} \right) + M e^{-\frac{t}{T_1^*}}$$

with

$$M_0^* = M_0 \frac{1 - ETR}{1 - ETR^*}$$

The total imaging time for the sequence is given by:

$$\text{time} = (TI + TD + \tau) * N_{pe2} * N_{segments}$$

where  $N_{pe2}$  is the number of phase encodes in the slab-select direction (the outer loop of the MP-RAGE sequence).

## References

- Barbier, E., Marrett, S., Danek, A., Vortmeyer, A., van, G.P., Duyn, J., Bandettini, P., Grafman, J., Koretsky, A., 2002. Imaging cortical anatomy by high-resolution MR at 3.0 T: detection of the stripe of Gennari in visual area 17. *Magn. Reson. Med.* 48, 735–738.
- Barth, M., Norris, D.G., 2007. Very high-resolution three-dimensional functional MRI of the human visual cortex with elimination of large venous vessels. *NMR Biomed.* 20, 477–484.
- Bock, N.A., Kocharyan, A., Liu, J.V., Silva, A.C., 2009. Visualizing the entire cortical myelination pattern in marmosets with magnetic resonance imaging. *J. Neurosci. Methods* 185, 15–22.
- Bock, N.A., Hashim, E., Kocharyan, A., Silva, A.C., 2011. Visualizing myeloarchitecture with magnetic resonance imaging in primates. *Ann. N.Y. Acad. Sci.* 1225, E171–E181.
- Bridge, H., Clare, S., Jenkinson, M., Jezzard, P., Parker, A.J., Matthews, P.M., 2005. Independent anatomical and functional measures of the V1/V2 boundary in human visual cortex. *J. Vis.* 5, 93–102.
- Brodman, K., 1909. Vergleichende lokalisationslehre der grosshirnrinde in ihren prinzipien dargestellt auf grund des zellenbaues. Barth.
- Campbell, A., 1905. *Histological Studies on the Localisation of Cerebral Function*. Cambridge University Press.
- Carmichael, D.W., Thomas, D.L., De Vita, E., Fernández-Seara, M.A., Chhina, N., Cooper, M., Sunderland, C., Randell, C., Turner, R., Ordidge, R.J., 2006. Improving whole brain structural MRI at 4.7 Tesla using 4 irregularly shaped receiver coils. *Neuroimage* 32, 1176–1184.
- Clare, S., Bridge, H., 2005. Methodological issues relating to in vivo cortical myelography using MRI. *Hum. Brain Mapp.* 26, 240–250.
- Clark, V.P., Courchesne, E., Grafe, M., 1992. In vivo myeloarchitectonic analysis of human striate and extrastriate cortex using magnetic resonance imaging. *Cereb. Cortex* 2, 417–424.
- Cohen-Adad, J., Polimeni, J.R., Helmer, K.G., Benner, T., McNab, J.A., Wald, L.L., Rosen, B.R., Mainero, C., 2012. T(2)\* mapping and B(0) orientation-dependence at 7 T reveal cyto- and myeloarchitecture organization of the human cortex. *Neuroimage* 60, 1006–10014.
- Deichmann, R., Good, C., Josephs, O., Ashburner, J., Turner, R., 2000. Optimization of 3-D MP-RAGE sequences for structural brain imaging. *Neuroimage* 12, 112–127.
- Deichmann, R., Schwarzbauer, C., Turner, R., 2004. Optimisation of the 3D MDEFT sequence for anatomical brain imaging: technical implications at 1.5 and 3 T. *Neuroimage* 21, 757–767.
- Elliott Smith, G., 1907. A new topographical survey of the human cerebral cortex, being an account of the anatomically distinct cortical areas and their relationship to the cerebral sulci. *J. Anat.* 41, 237–254.
- Fischl, B., Dale, A.M., 2000. Measuring the thickness of the human cerebral cortex from magnetic resonance images. *Proc. Natl. Acad. Sci. U. S. A.* 97, 11050–11055.
- Fukunaga, M., Li, T., van Gelderen, P., de Zwart, J.A., Shmueli, K., Yao, B., Lee, J., Maric, D., Aronova, M.A., Zhang, G., Leapman, R.D., Schenck, J.F., Merkle, H., Duyn, J.H., 2010. Layer-specific variation of iron content in cerebral cortex as a source of MRI contrast. *Proc. Natl. Acad. Sci. U. S. A.* 107, 3834–3839.
- Geyer, S., Weiss, M., Reimann, K., Lohmann, G., Turner, R., 2011. Microstructural parcellation of the human cerebral cortex – from Brodmann's post-mortem map to in vivo mapping with high-field magnetic resonance imaging. *Front. Hum. Neurosci.* 5, 19.
- Glasser, M.F., Van Essen, D.C., 2011. Mapping human cortical areas in vivo based on myelin content as revealed by T1- and T2-weighted MRI. *J. Neurosci.* 31, 11597–11616.
- Hopf, A., 1955. Über die Verteilung myeloarchitektonischer Merkmale in der isokortikalen Schläfenlappenrinde beim Menschen. *J. Hirnforsch.* 2, 36–54.
- Hopf, A., 1956. Über die Verteilung myeloarchitektonischer Merkmale in der Stirnhirnrinde beim Menschen. *J. Hirnforsch.* 2, 311–333.
- Hopf, A., 1968. Photometric studies on the myeloarchitecture of the human temporal lobe. *J. Hirnforsch.* 10, 285–297.
- Hopf, A., 1970. Photometric studies on the myeloarchitecture of the human parietal lobe. II. Postcentral region. *J. Hirnforsch.* 12, 135–141.
- Hopf, A., Vitzthum, H.G., 1957. Über die Verteilung myeloarchitektonischer Merkmale in der Scheitellappenrinde beim Menschen. *J. Hirnforsch.* 3, 79–104.
- Katscher, U., Börner, P., 2006. Parallel RF transmission in MRI. *NMR Biomed.* 19, 393–400.
- Kim, E.Y., Kim, D., Chang, J., Yoo, E., Lee, J., Park, H., 2009. Triple-layer appearance of Brodmann area 4 at thin-section double inversion-recovery MR imaging. *Radiology* 250, 515–522.
- Li, W., Wu, B., Avram, A.V., Liu, C., 2012. Magnetic susceptibility anisotropy of human brain in vivo and its molecular underpinnings. *Neuroimage* 59, 2088–2097.
- Lichy, M.P., Wietek, B.M., Mugler III, J.P., Horger, W., Menzel, M.I., Anastasiadis, A., Siegmann, K., Niemeier, T., Königsrainer, A., Kiefer, B., Schick, F., Claussen, C.D., Schlemmer, H., 2005. Magnetic resonance imaging of the body trunk using a single-slab, 3-dimensional, T2-weighted turbo-spin-echo sequence with high sampling efficiency (SPACE) for high spatial resolution imaging: initial clinical experiences. *Invest. Radiol.* 40, 754–760.
- Lu, H., Nagae-Poetscher, L.M., Golay, X., Lin, D., van Pomper, M., Zijl, P.C.M., 2005. Routine clinical brain MRI sequences for use at 3.0 Tesla. *J. Magn. Reson. Imaging* 22, 13–22.
- Marques, J.P., Kober, T., Krueger, G., van der Zwaag, W., Van de Moortele, P., Gruetter, R., 2010. MP2RAGE, a self bias-field corrected sequence for improved segmentation and T1-mapping at high field. *Neuroimage* 49, 1271–1281.
- Mugler III, J.P., Brookeman, J.R., 1990. Three-dimensional magnetization-prepared rapid gradient-echo imaging (3D MP RAGE). *Magn. Reson. Med.* 15, 152–157.
- Sánchez-Panchuelo, R.M., Francis, S.T., Schluppeck, D., Bowtell, R.W., 2012. Correspondence of human visual areas identified using functional and anatomical MRI in vivo at 7 T. *J. Magn. Reson. Imaging* 35, 287–299.
- Sigalovsky, I.S., Fischl, B., Melcher, J.R., 2006. Mapping an intrinsic MR property of gray matter in auditory cortex of living humans: a possible marker for primary cortex and hemispheric differences. *Neuroimage* 32, 1524–1537.
- Trampel, R., Ott, D.V.M., Turner, R., 2011. Do the congenitally blind have a stria of Gennari? First intracortical insights in vivo. *Cereb. Cortex* 21, 2075–2081.
- Van de Moortele, P., Auerbach, E.J., Olman, C., Yacoub, E., Uğurbil, K., Moeller, S., 2009. T1 weighted brain images at 7 Tesla unbiased for proton density, T2\* contrast and RF coil receive B1 sensitivity with simultaneous vessel visualization. *Neuroimage* 46, 432–446.
- Van Essen, D.C., Drury, H.A., Dickson, J., Harwell, J., Hanlon, D., Anderson, C.H., 2001. An integrated software suite for surface-based analyses of cerebral cortex. *J. Am. Med. Inform. Assoc.* 8, 443–459.
- Vogt, C., Vogt, O., 1919. Allgemeinere ergebnisse unserer hirnforschung. *J. Psychol. Neurol.* 25, 279–461.
- Voigt, T., Nehrke, K., Doessel, O., Katscher, U., 2010. T1 corrected B1 mapping using multi-TR gradient echo sequences. *Magn. Reson. Med.* 64, 725–733.
- Walters, N.B., Egan, G.F., Kril, J.J., Kean, M., Waley, P., Jenkinson, M., Watson, J.D.G., 2003. In vivo identification of human cortical areas using high-resolution MRI: an approach to cerebral structure–function correlation. *Proc. Natl. Acad. Sci. U. S. A.* 100, 2981–2986.
- Wang, J., Qiu, M., Constable, R., 2005. In vivo method for correcting transmit/receive nonuniformities with phased array coils. *Magn. Reson. Med.* 53, 666–674.
- Wansapura, J.P., Holland, S.K., Dunn, R.S., Ball, W.S.J., 1999. NMR relaxation times in the human brain at 3.0 Tesla. *J. Magn. Reson. Imaging* 9, 531–538.
- Weiss, M., Geyer, S., Lohmann, G., Trampel, R., Turner, R., 2010. Longitudinal relaxation time T1 as a guide to in-vivo myeloarchitecture. *Proceedings of the 16th Annual Meeting of the Organization for Human Brain Mapping*, p. 134.
- Woods, R.P., Dapretto, M., Sicotte, N.L., Toga, A.W., Mazziotta, J.C., 1999. Creation and use of a Talairach-compatible atlas for accurate, automated, nonlinear intersubject registration, and analysis of functional imaging data. *Hum. Brain Mapp.* 8, 73–79.
- Zhu, D.C., Penn, R.D., 2005. Full-brain T1 mapping through inversion recovery fast spin echo imaging with time-efficient slice ordering. *Magn. Reson. Med.* 54, 725–731.
- Zilles, K., Zilles, K., Amunts, K., 2012. *Architecture of the cerebral cortex. The Human Nervous System*. Academic Press.